공학석사학위논문

Experimental and Numerical Feasibility Study on Application of Electric Pump Cycle in Small Rocket Engine

소형 로켓엔진에서 전기펌프 사이클 적용에 대한 실험 및 수치적 타당성 연구

2022 년 2 월

서울대학교 대학원

항공우주공학과

박 연 규

소형 로켓엔진에서 전기펌프 사이클 적용에 대한 실험 및 수치적 타당성 연구

Experimental and Numerical Feasibility Study on Application of Electric Pump Cycle in Small Rocket Engine

지도교수 윤 영 빈

이 논문을 공학석사 학위논문으로 제출함

2022 년 2 월

서울대학교 대학원

항공우주공학과

박 연 규

박연규의 공학석사 학위논문을 인준함

2022 년 2 월

위 원 장 여 재 익

부위원장 윤 영 빈

위 원 이 복 직

Abstract

As the miniaturization of satellites and the use of satellite constellation increase, the demand for small launch vehicles is also increasing. Accordingly, numerous private companies are developing and operating small launch vehicles, and in particular, the number of small launch vehicles which applying the electric pump cycle, is increasing. The electric pump cycle is a propellant feed system that drives a pump using an electric motor, unlike a gas generator cycle that drives the pump with a gas turbine. Many studies have been conducted to evaluate the performance of the electric pump cycle compared to other propellant feed systems based on the mass modeling. However, no study has been conducted to validate the application of the electric pump cycle in small rocket engines with thrust level of 10 kN or less. In this study, the validity of the application of the electric pump cycle was dealt with in an experimental and numerical method. First, a cryogenic performance test using liquid nitrogen as simulants was conducted using a cryogenic electric pump system for a 5.4 kN class pintle rocket engine. From the numerical analysis and cryogenic performance test results, the successful operation of the electric pump under the cryogenic

environment was validated. Second, based on mass modeling, the performance of electric pump cycle, gas generator cycle and pressure-fed cycle was compared and analyzed. Small rocket engines with thrust level of 10 kN or less are characterized by very low specific speed of the pump due to small thrust level. In this study, mass modeling was performed in consideration of the hydraulic efficiency of the pump according to the specific speed. The performance of the propellant feed system according to the combustion pressure, thrust, and rotational speed conditions of the pump was compared for a small rocket engine. Under the conditions of combustion pressure of 10 bar, thrust level of 5.4 kN, and pump rotational speed of 28,000 RPM used in the experimental feasibility study, the performance of the electric pump cycle was higher than that of the other two propellant feed systems. Finally, this study numerically verified the feasibility of applying an electric pump cycle to a small rocket engine of 10 kN or less and experimentally verified that it would be possible to apply an electric pump cycle to a small rocket engine of 5.4 kN.

Keyword : Electric pump cycle, Liquid methane, Rocket engine, Cryogenic test, Numerical analysis, Performance evaluation,

Student Number : 2020-25188

Table of Contents

List of Tables

List of Figures

Chapter 1 INTRODUCTION

1.1 Study Background

Recently, government-led space development, which began in the Cold War era, has been changing to private-led space development. Private-led space development makes transport cost of payload cheaper while actively applying new technologies and concepts. For example, reuse of launch vehicles which uses re-ignition and engine throttling is rapidly decreasing the cost of payload transportation. In addition, with miniaturization of traditional large satellites, constellation mission containing as many as hundreds of small satellites is increasing. Representative examples of constellation mission using small satellites are SpaceX's Starlink and OneWeb's satellite internet network service. Small satellites have the advantage of being more economical in development period, manufacturing cost, and launch cost than large satellites, and their performance does not lag behind. Also, with increasing of small satellites market, the demand for small launch vehicles is also increasing.

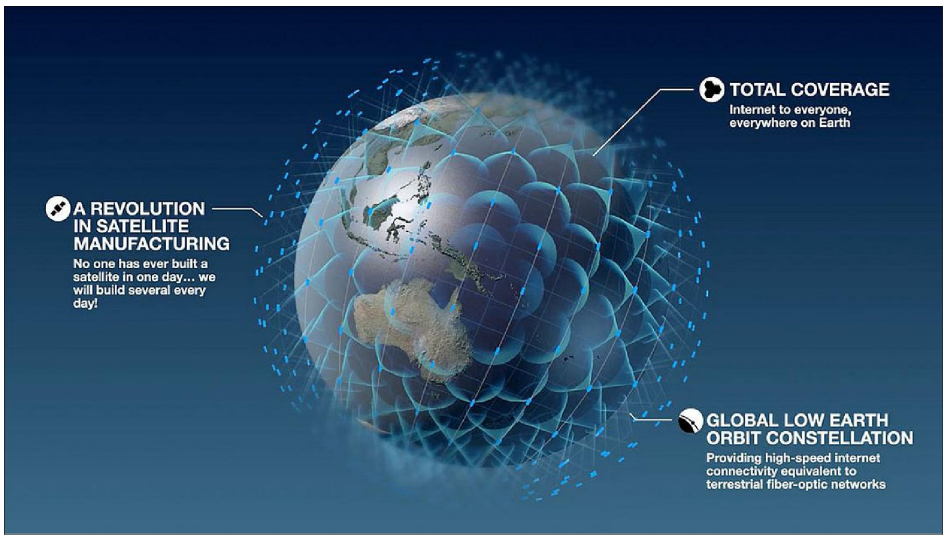

Figure 1.1 OneWeb's satellite internet network service

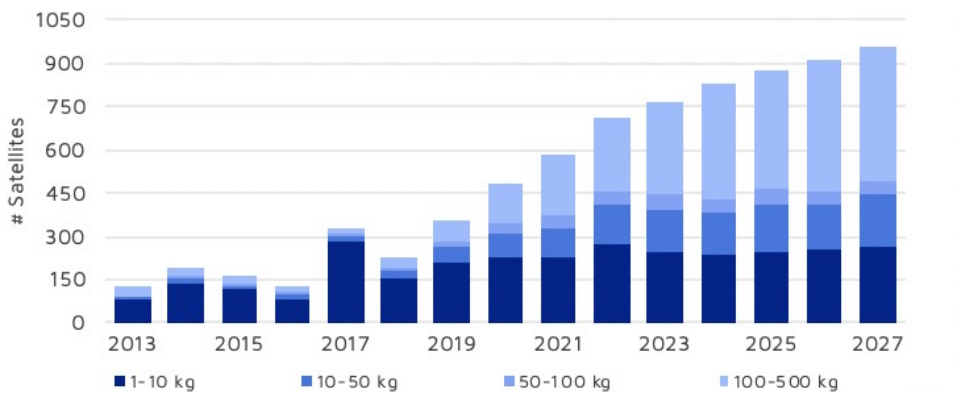

Figure 1.2 Global small satellites launches by mass category

Along with the above background, small launch vehicles with an electric pump (EP) cycle are attracting attention. The EP cycle is a propellant feed system that drives a pump using an electric motor, unlike a gas generator (GG) cycle that drives a pump using a gas turbine.

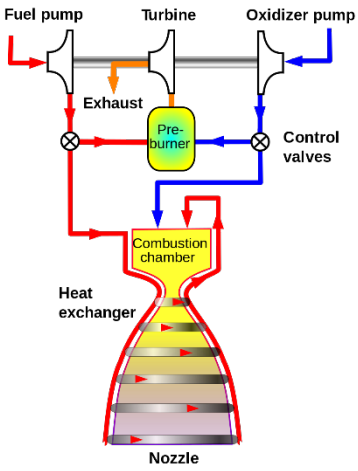

Figure 1.3 Gas generator cycle

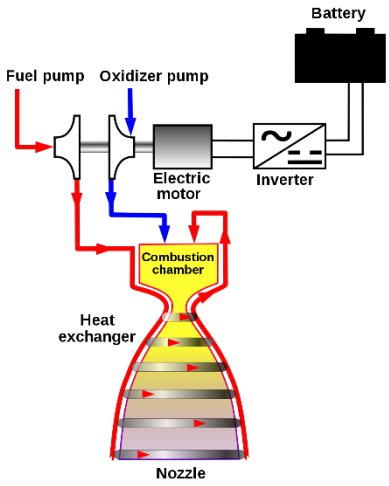

Figure 1.4 Electric pump cycle

The EP cycle has many advantages compared to the GG cycle. First, the EP cycle has advantages such as structurally simple, short research and development period, and low manufacturing cost [1]. Also, by using an electric motor, the controlling of the rotational speed of the pump has been simplified, which has made it easier to engine throttling. In the GG cycle, not only the combustion chamber but also the turbine and GG are exposed to high temperatures, but in the EP cycle, only the combustion chamber is exposed to high temperatures. The advantages of the EP as described above may lead to an increase in reliability of the rocket engine. In addition, due to the acceleration of the development of electric motor and battery technology due to the commercialization of electric vehicles and drones, the performance of

the EP cycle is improving. However, since the EP cycle has a disadvantage in that the inverter and the battery remain in a dry weight even after the combustion is finished, many studies have been conducted on the performance evaluation of the EP cycle through mass modeling.

As an advantage of such the EP cycle, many domestic and foreign companies develop and operate small launch vehicles to which the EP cycle is applied. Rocket Lab applied it to a 25kN Rutherford engine, was the only company currently carrying out commercial launches, and most recently Astra Space succeeded in launching its first commercial launch. In addition, there are venture orbital systems, Copenhagen Suborbitals, and Deep Blue Aerospace, and what they have in common is that they have a thrust range between 20kN and 100kN overall. In Korea, InnoSpace has applied the EP cycle to feed oxidizer for a 150 kN-class hybrid rocket engine.

Figure 1.5 Rutherford engine of Electron, Rocket Lab

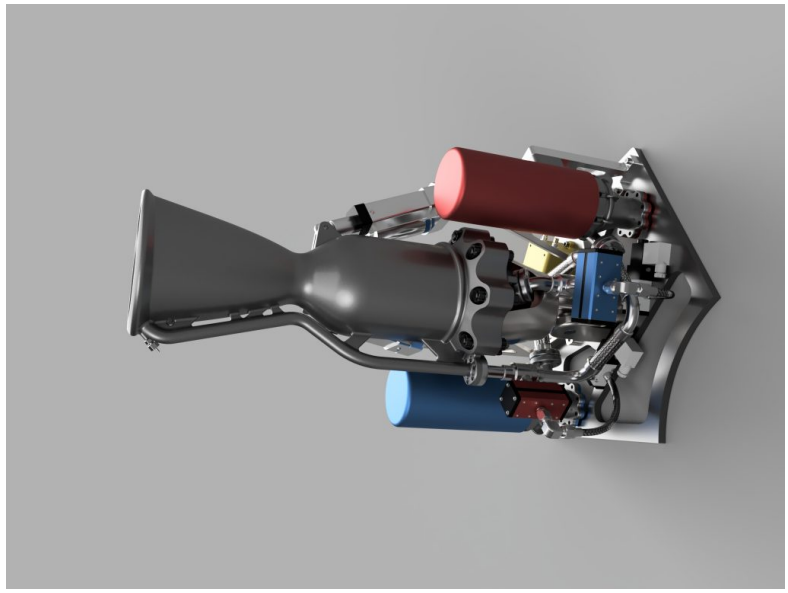

Figure 1.6 Navier engine of Zephyr, Venture Orbital Systems

1.2 Previous studies

Kwak et al. compared the EP cycle and the GG cycle based on mass modeling [2]. It was revealed that the longer the combustion time of the rocket engine and the lower the combustion chamber pressure, the better the performance of the EP cycle. In addition, when the EP cycle was applied to the 3rd stage of the KSLV-II, the payload weight was lower than when the GG cycle was applied under the same conditions, but the payload weight was higher under the lower combustion chamber pressure conditions.

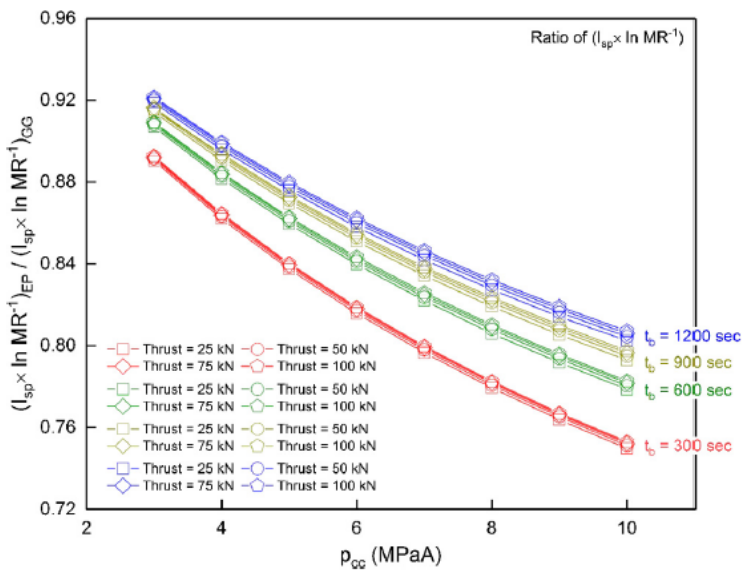

Figure 1.7 Ratio of (I_{sp} x ln MR^{-1}) of EP cycle to GG cycle

Lee et al. compared the EP cycle and the GG cycle for small rocket engine with 500 kN [3]. Cui et al. compared the EP cycle and staged combustion cycle based on both pressure loss model and mass model [4]. Liang et al. proposed a novel electric expander cycle in which an EP cycle and an expander cycle are mixed [5]. In the proposed electric expander cycle, the EP cycle and the expander cycle were used for the fuel feed system and oxidizer feed system, respectively. The pump of expander cycle was driven by a turbine which uses vaporized fuel, GCH4. The main characteristic of this system is the relatively independent pressurization system which makes controlling the mixture ratio and throttling easier.

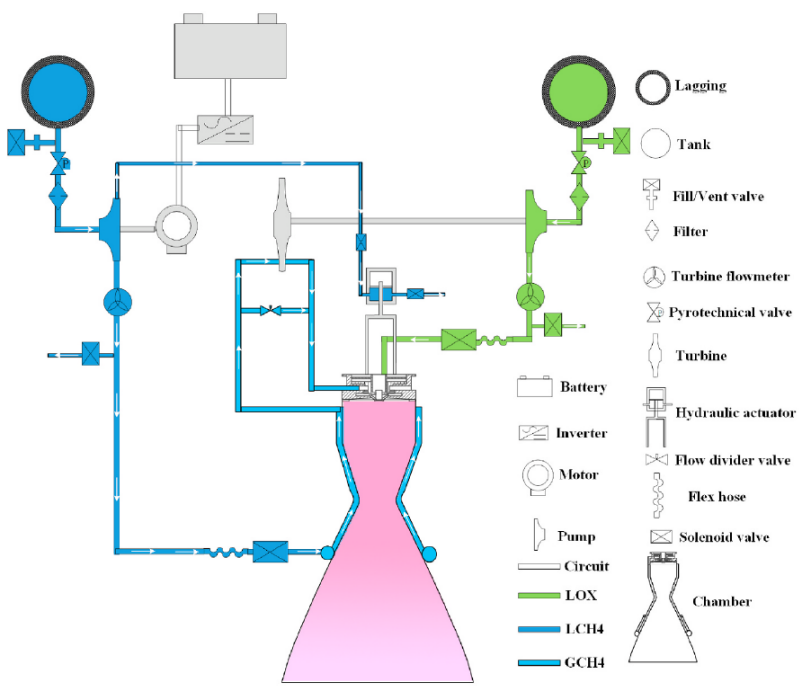

Figure 1.8 The electric expander cycle system scheme

Casalino et al. compared the EP cycle and pressure-fed cycle for a hybrid rocket engine [6]. Rachov et al. evaluated the performance of the EP cycle, the GG cycle and pressure-fed cycle [7]. Yoon designed the EP based on the 5.4 kN-class liquid methane pintle engine [8]. Two impellers with different discharge angle, the type A impeller with discharge angle of 10° and the type B impeller with discharge angle of 33°, were designed.

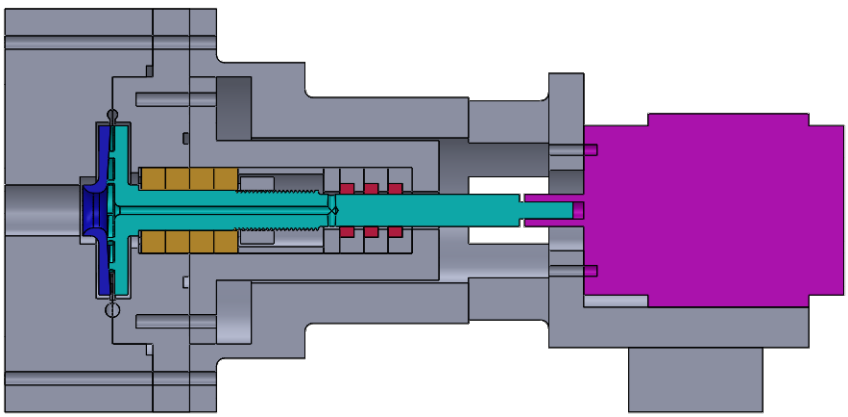

Figure 1.9 Configuration of the electric pump

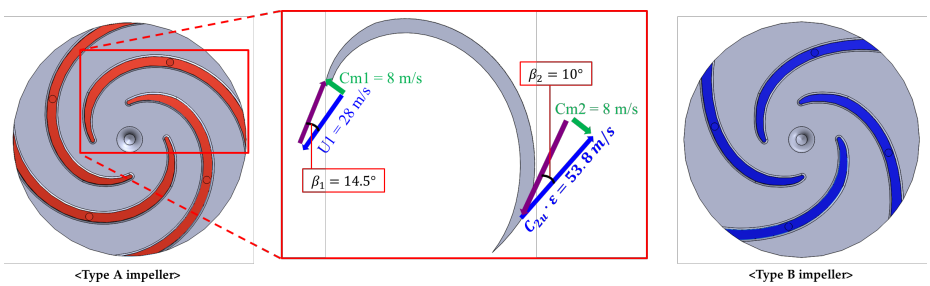

Figure 1.10 Two impellers with different discharge angle

Kim conducted the cold-water performance test using aforementioned two impellers which designed by Yoon [9]. Both hydraulic and suction performance were conducted. In the hydraulic performance test, the type A impeller shows higher efficiency than the type B impeller. In the suction performance test, the type B impeller is more vulnerable to cavitation than the type A impeller [10].

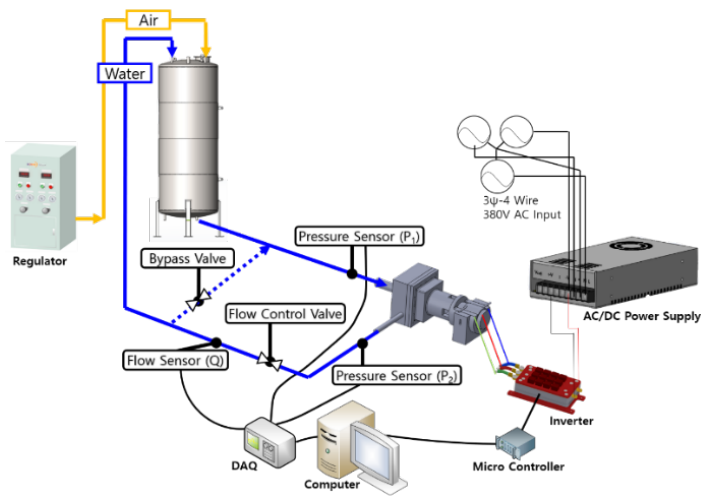

Figure 1.11 Schematic of pump test rig

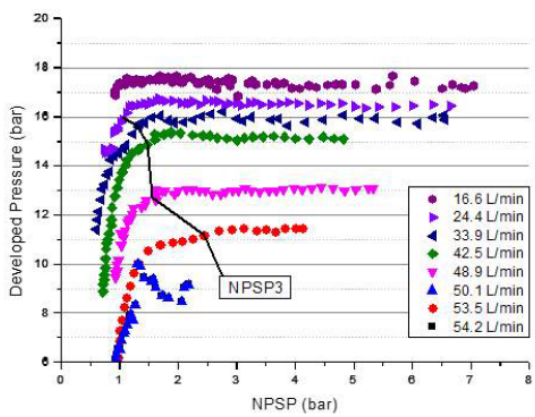

Figure 1.12 Suction performance test data

1.3 Purpose of research

Previous studies have not demonstrated electric pumps for small rocket engines, such as design/test/evaluation, and only studies have been conducted on system performance evaluation. In addition, only engines of class 30 kN or higher have been studied, and there is no comparison of performance of gas generator cycles, pressurized cycles, electric pump cycles, and three cycles that may be used as supply systems for small engines. The purpose of this study is a total of two. The possibility of utilization of the electric pump is confirmed by comparing the performance of an electric pump cycle, a gas generator cycle, and a pressurized cycle in a low thrust engine of 10 kN or less. The second is the design of a cryogenic pump system based on the results of the water flow test conducted with room temperature water and the verification of the pump design through a performance test using liquid nitrogen.

Chapter 2 EXPERIMENTAL VALIDATION

2.1 Electric pump design

The EP cycle used in this study was designed based on a 5.4 kN-class pintle methane engine. Table 2.1 shows the specification of the pintle methane engine.

Table 2.1 Pintle engine specification

Parameter	Value	Unit
Fuel	LCH4	-
Oxidizer	LOX	-
I_{sp}	310	s
O/F Ratio	3.44	-
Fuel mass flow rate	0.4	kg/s
Thrust	5395	N
Combustion chamber pressure	10	bar
Injector pressure loss	8	bar
Pump outlet pressure	18	bar

Considering 10 bar of the combustion chamber pressure and 8 bar of pressure loss in injector and feed line, the discharge pressure of the pump is 18 bar. The suction pressure of the pump is assumed to be 3 bar to prevent cavitation. Therefore, the design condition of the pump is 15 bar of developed pressure. Pump design was made by

setting the available rotational speed of the commercial BLDC motor, 28000 RPM. Table 2.2 shows the specification of the electric pump.

Table 2.2 Electric pump specification

Parameter	Value	Unit
Fluid	LCH4	-
Mass flow rate	0.4	kg/s
Density	442.4	kg/m^3
Inlet pressure	3	bar
Outlet pressure	18	bar
Developed pressure	15	bar
Developed head	346	m
Rotational speed	28,000	RPM

Figure 2.1 shows the schematic of the EP system which contains mechanical components and electrical components. Figure 2.2 presents the real EP with the electric motor.

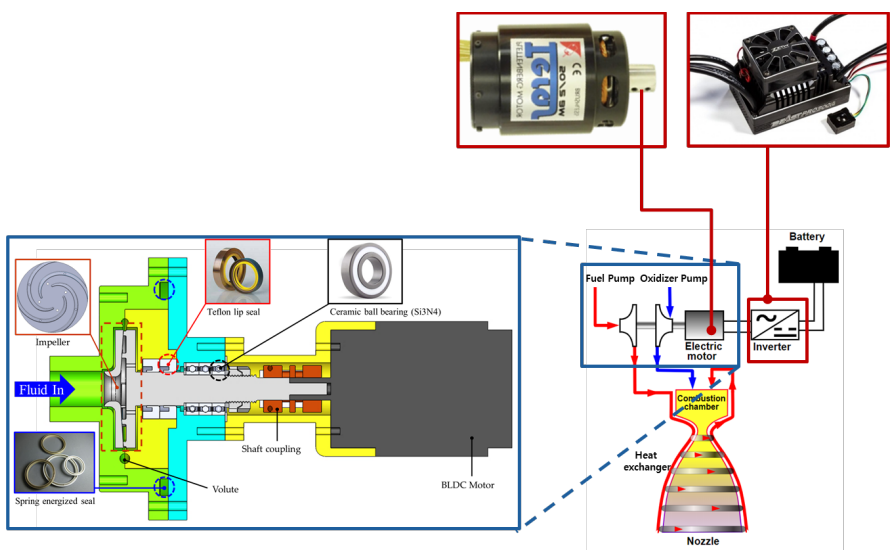

Figure 2.1 Schematic of the electric pump system

Figure 2.2 Real electric pump with the electric motor

2.1.2 Mechanical components

Figure 2.3 presents the schematic of cryogenic pump system. Mechanical components include the impeller, volute, seals, and bearings.

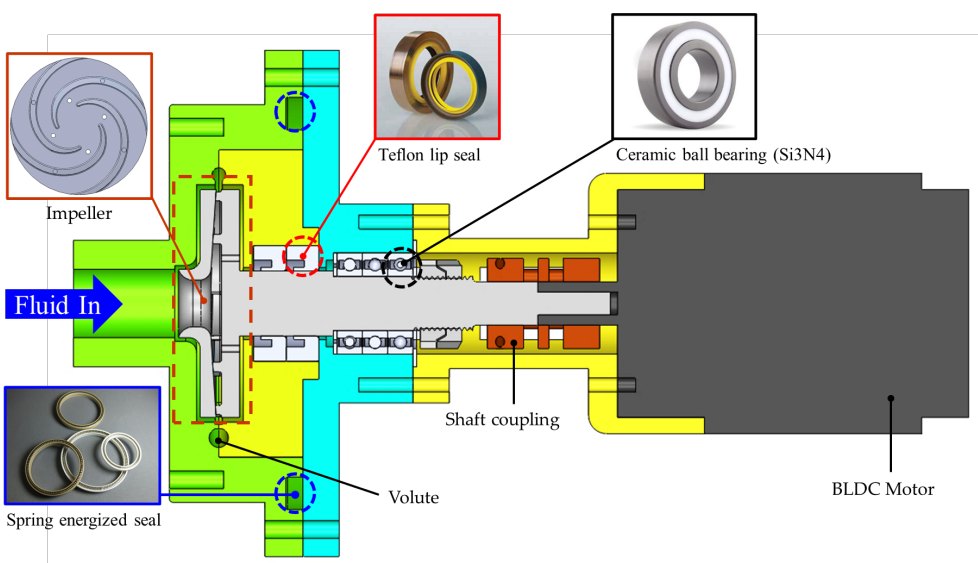

Figure 2.3 Schematic of mechanical components of the cryogenic pump

In the previous studies, we used the spring energized seal with the rubber case as the rotational seal and the rubber O-ring as the static seal. However, in this study, in consideration of the cryogenic environment, Teflon lip seal and PTFE spring energized seal were used as rotational seals and static seals, respectively. Bearing also used ceramic ball bearings. Table 2.3 presents seals and bearings used in previous study and this study.

Table 2.3 Seals and bearings used in previous study and this study

Components	Water pump (Previous study)	Cryogenic pump
Rotational seal	Rubber spring energized seal	Teflon lip seal
Static seal	Rubber O-ring	PTFE spring energized seal
Bearing	Stainless-ceramic hybrid ball bearing	Full ceramic ball bearing (Si_3N_4)

The characteristic of the rotating seal in this study is a very high surface speed of 26 m/s. Rotating seals available in cryogenic environments are mechanical seals, spring energized seals, and Teflon lip seals. Figure 2.4 shows a mechanical face seal which commonly used in turbopumps are high-performance. However, it is difficult to obtain commercial products. Figure 2.5 and Figure 2.6 show the P-V chart of a spring energized seal and Teflon lip seal, respectively. Spring energized seals have a maximum surface speed of 10 m/s, which does not meet the requirements. Finally, we selected a Teflon lip seal that is inexpensive and operates at a surface speed of 45 m/s.

Figure 2.4 Mechanical face seal

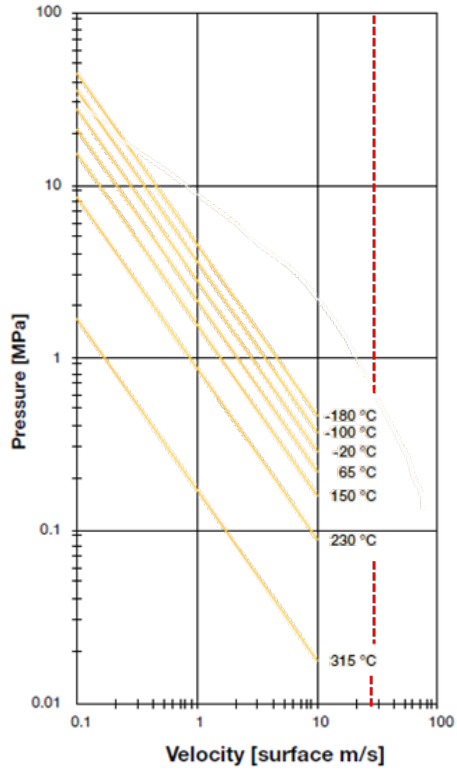

Figure 2.5 P-V chart of spring energized seal

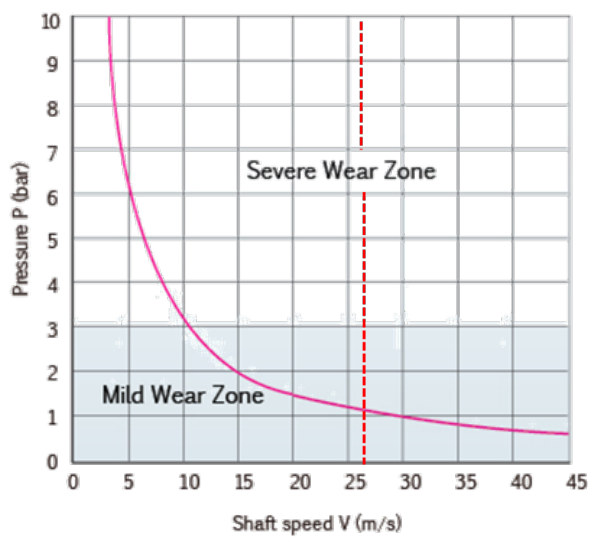

Figure 2.6 P-V chart of Teflon lip seal

The rubber O-ring, a static seal used in the previous study, is not suitable for cryogenic environments. Figure 2.7 shows static seals suitable for cryogenic environment including conical seals, spring-energized PTFE seals, and spring-energized C-ring seals. Conical seals have disadvantages that it is difficult to obtain commercial products. The C-ring seal has the best sealing performance. However, there is a high risk of failure due to many design variables to consider and has the disadvantage that it cannot be reused due to characterizes of metal materials. The sealing performance is lower than that of the C-ring seal, but the spring-energized PTFE seal, which is high enough, can be reused within the appropriate level and is not difficult to design. Thus, the spring-energized PTFE seal is selected for static sealing.

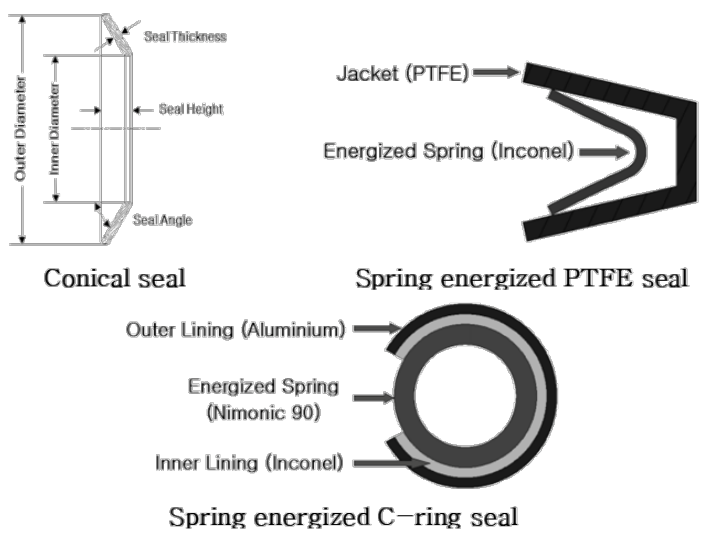

Figure 2.7 Static seals suitable for cryogenic environment

In this study, the type A impeller with discharge angle of 10º was used. Balance hole was changed from the previous study. As shown in Figure 2.8, former balance hole needs large volume. Therefore, by changing the balance hole as shown in Figure 2.9, the mass reduced about 70%.

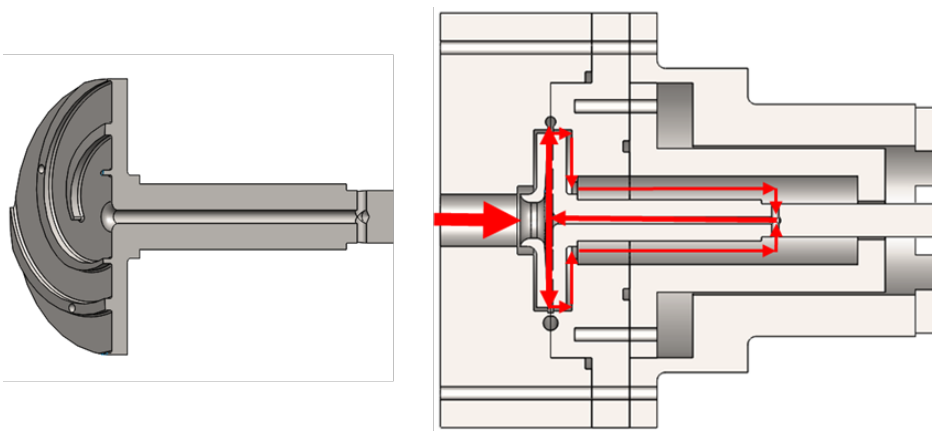

Figure 2.8 Former balance hole

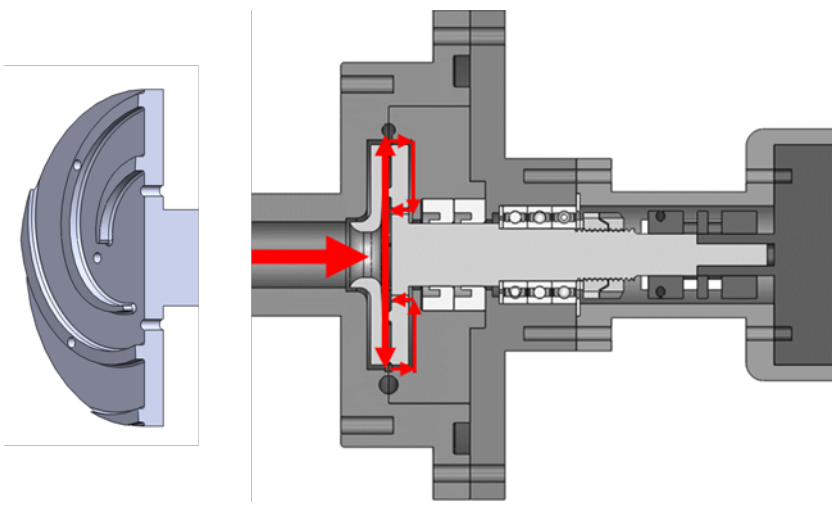

Figure 2.9 Balance hole in this study

2.1.3 Electrical components

Table 2.4 and Figure 2.10 present details of electrical components and the schematic of electrical components of the system, respectively. The power supply converts and supplies three-phase 380V AC power into 36V DC power, and the inverter controls frequency and voltage to control the rotational speed of the motor. In general, a permanent magnet synchronous motor and a brushless direct current motor were used for the EP cycle [11]. In this study, the brushless direct current motor was used. Inverters and motors used compact commercial products for drones and RC cars, not industrial products.

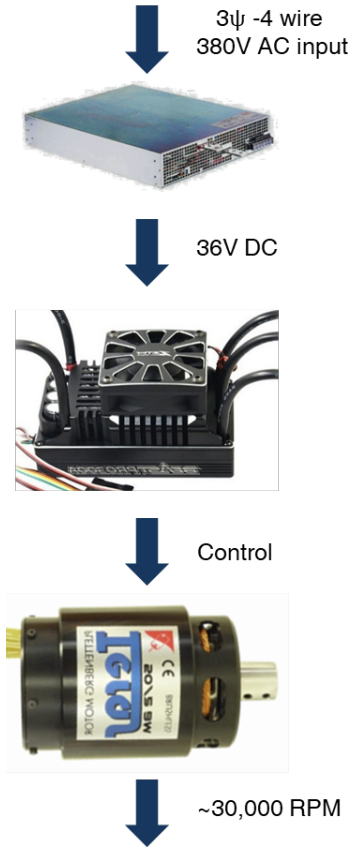

Figure 2.10 Electrical components of the system

Table 2.4 Details of electrical components

Components	Input	Output
Power supply *Meanwell*	3ψ -4 wire 380V AC	36V DC (Max. current: 270A)
Inverter *ZTW*	36V DC (22.2V - 44.4V)	36V DC (Max. current:300A)
BLDC motor *Plettenberg*	36V DC (37V - 51.8V)	950 RPM/Volt (Max. RPM: 30,000)

2.2 Numerical method

In this study, numerical analysis was performed using ANSYS CFX, and the analysis of hydraulic performance is covered. A steady-state analysis was performed, and the target fluid is cold-water, liquid nitrogen, and liquid methane. The boundary conditions were pressure inlet conditions and mass flow outlet conditions. Table 2.5 shows the condition of numerical analysis.

Table 2.5 Numerical analysis condition

Analysis type		Steady state
Fluid		Cold water(20℃), LN2, LCH4
Turbulence model		SST k-omega
Boundary condition		Mass flow outlet Pressure inlet
Slip condition		Free slip wall
Mesh	Type	Polyhedral
	Number of elements	1,861,972
	Inflation layer	5

₩

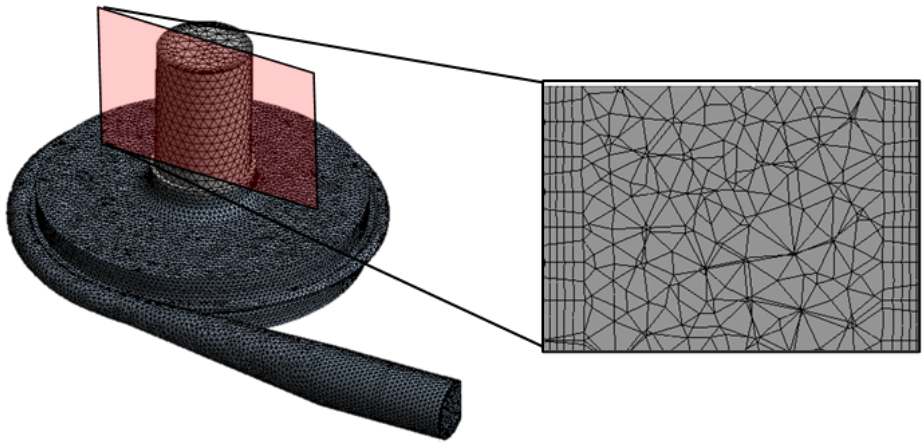

Figure 2.11 Meshed model and inflation layer

The developed pressure was calculated as the difference between the pressure at the outlet and the pressure at the inlet. Figure 2.12 presents 3-D pressure contour. Numerical analysis was performed at 14000, 18000, and 22000 RPM for comparison with the results of the cold-water test of previous study.

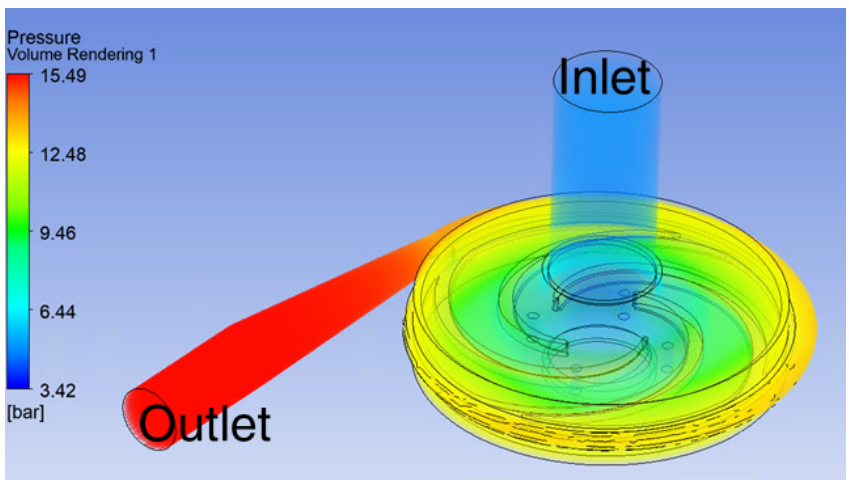

Figure 2.12 3-D pressure contour

Figure 2.13 shows the comparison between CFD results and cold-water test. Considering that the accuracy of pump rotation speed in the test environment is ±2%, it could be determined that the numerical analysis result is similar with the test result.

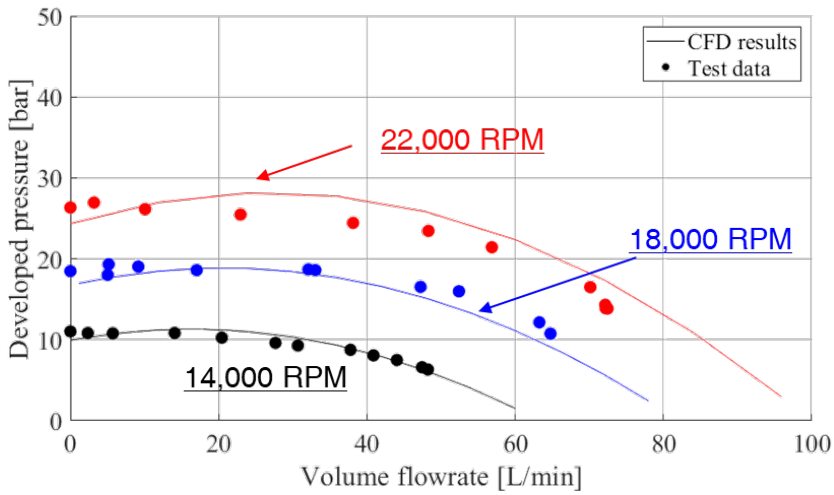

Figure 2.13 Comparison between CFD results and cold-water test

As shown in Figure 2.14, Axial thrust is generated due to the pressure difference generated at the front and rear ends of the impeller when the pump is driven. Because axial force reduces the life of the system, the balance hole is used for reducing the axial force. The pressure difference between the front and rear ends of the impeller is decreasing by the balance hole.

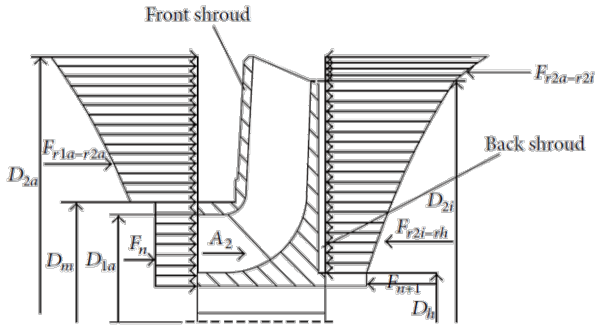

Figure 2.14 Distribution of axial thrust on one impeller

Based on the numerical analysis, the axial force was calculated using the pressure distribution was divided by area in the front and rear planes of the impeller. When the balance hole of the previous study was used, the axial force was 191.1N, but it decreased by about 3% to 185.5N through the improvement of the balance hole. Figure 2.15 shows the pressure contour inside the pump.

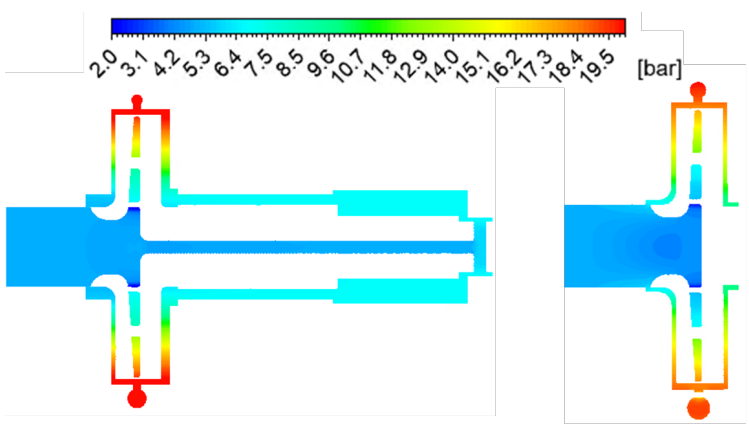

(a) Before change (b) After change

Figure 2.15 Pressure contour inside pump

2.3 Experimental method

2.3.1 Test facility

Figure 2.16 shows the schematic of the test facility. In this test facility, a cryogenic tank was directly connected to the pump system, and a liquid nitrogen tank for cooling and a nitrogen tank for a testing were used separately. In the test start stage, the cooling tank was opened until the pipe is sufficiently cooled. Then, the cooling tank was closed, and testing tank was opened. The testing tank was maintained at a pressure of about 10 bar before opening, and data were obtained by driving the pump when the system reached a steady state after opening. Flow control was performed by adjusting the ball valve located at the rear end of the pump. The sensor used a turbine flow meter and a pressure transducer at the inlet end, a T-type thermocouple, and a pressure transducer and a T-type thermocouple at the outlet end. The pump rotational speed was measured using a tachometer. Figure 2.17 shows the real cryogenic performance test facility.

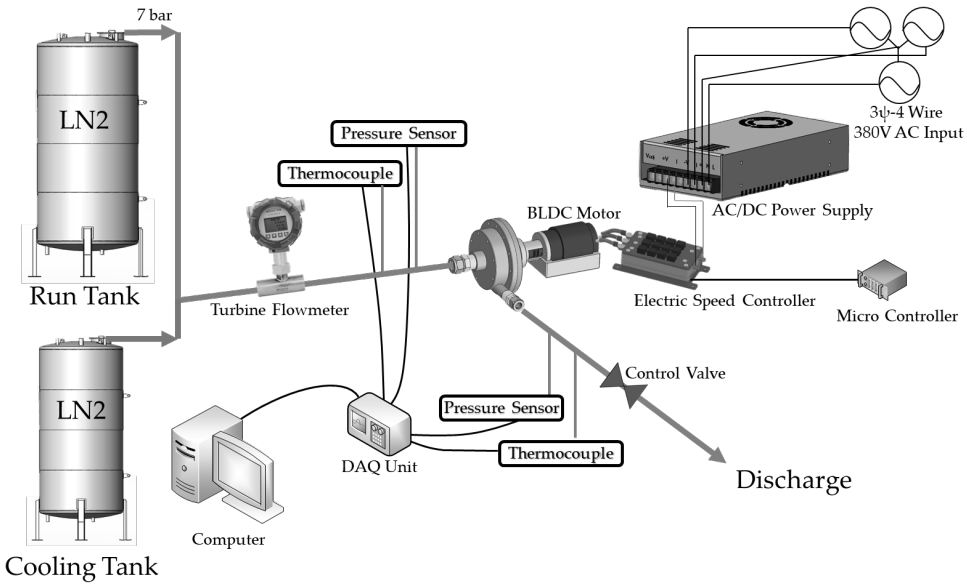

Figure 2.16 Schematic of cryogenic performance test facility

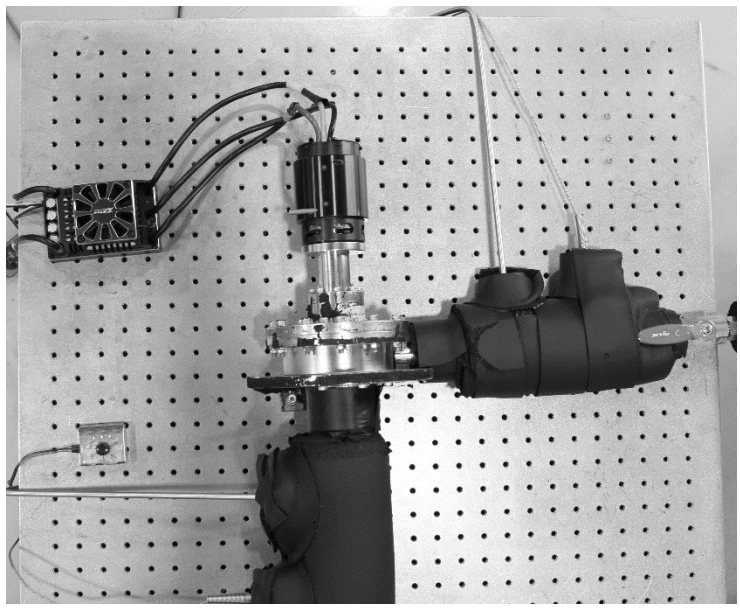

Figure 2.17 Cryogenic performance test facility

2.3.2 Test condition

With same impeller diameter, depending on the pump rotational speed, the flow rate developed pressure can be correlated through the following equation. From the results of the cold-water test of the previous studies, it was verified that the affinity law of the pump was well established.

$$\frac{Q_1}{Q_2} = \frac{N_1}{N_2}$$

$$\frac{\Delta P_1}{\Delta P_2} = \left(\frac{N_1}{N_2}\right)^2$$

Because heat generation of electrical components (motor, inverter, harness) increases as rotational speed increases, the tests were performed only at 10000 RPM and 14000 RPM in this study. Table 2.6 shows the cryogenic performance test condition

Table 2.6 Cryogenic performance test condition

Test condition	
Rotational speed	10000 RPM 14000 RPM
Suction pressure	5 bar
Outlet pressure	0 bar (P_{atm})

Figure 2.18 and Figure 2.19 show one of the 14,000 RPM cryogenic performance tests and results, respectively. Data post-processing used a kernel filter, and the rotational speed was slowly

increased over about 30 seconds. In addition, the electric motor was operated at the final rotational speed for about 20 seconds to reach a steady state in consideration of the sampling time of the flow meter.

Figure 2.18 One of the 14,000 RPM cryogenic performance tests

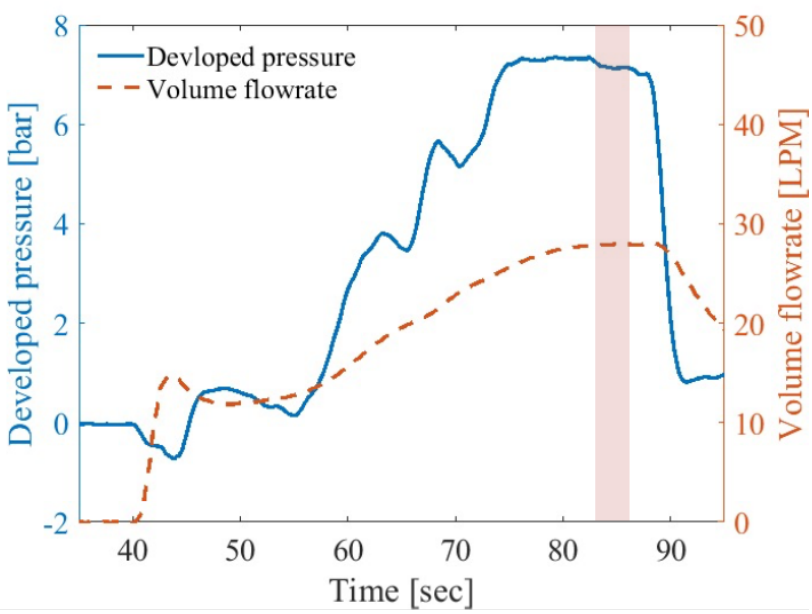

Figure 2.19 One of the cryogenic performance test results

2.4 Results and discussion

The results shown through experimental data and numerical analysis are shown in Figure 2.20. The overall trend is similar, but it seems necessary to correct the numerical analysis model such as slip conditions. In addition, it is necessary to conduct additional experiments to improve reliability of test results. The feature of this experiment is that the data in the low flow section below 15 LPM is not valid. Due to the limitations of the insulation and cooling performance of this system, sufficient cooling was not achieved in the low flow section, and it was confirmed that the pump's performance rapidly decreased due to a mixture of liquid and gas phases.

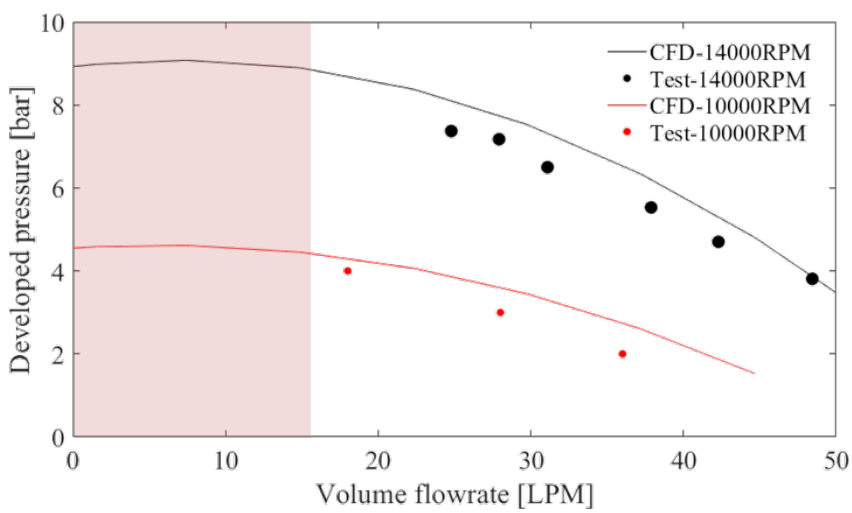

Figure 2.20 CFD results and test data for LN2

Numerical analysis modeling was performed based on the results of performance tests performed with water and liquid nitrogen

at room temperature, and pump performance was predicted in liquid methane, a real medium. Table 2.7 shows the performance comparison between CFD results and design point. As a result of CFD prediction, a pressure increase of 15.28 bar was made at the design flow rate of 54LPM, which was a very slight difference between the design pressure increase of 15 bar and 1.87%. Figure 2.21 shows CFD results and design point for real-propellant, LCH4.

Table 2.7 Performance comparison between CFD results and design point

	CFD	Design point	Error (%)
Developed pressure (bar)	15.28	15.00	1.87

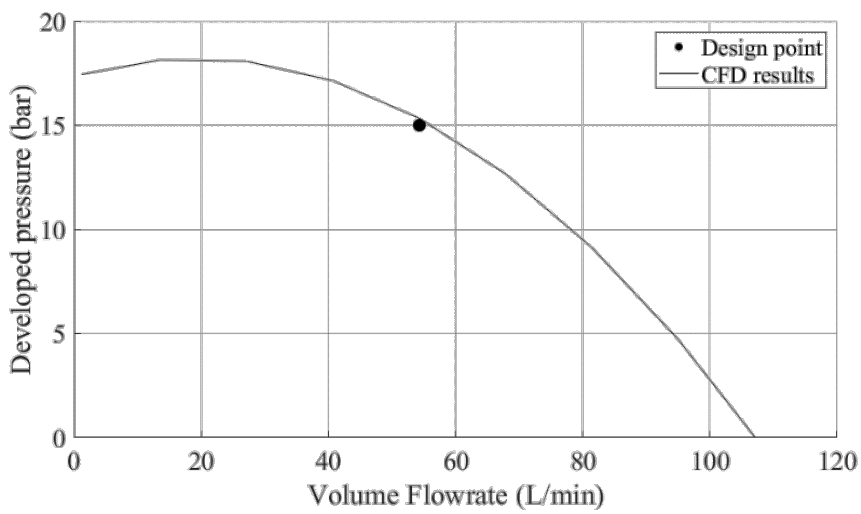

Figure 2.21 CFD results and design point for LCH4 (N = 28,000 RPM)

Chapter 3 PERFORMANCE EVALUATION

The mass modeling for the GG cycle, EP cycle and pressure-fed cycle is reported in numerous studies. In this chapter, a novel mass modeling was described considering the pump efficiency according to specific speed of the pump.

3.1 Gas generator cycle

Mass modeling of the components constituting the propellant feed system must be performed to evaluate the performance of the feed system. The mass modeling of the GG cycle is shown as Figure 3.1. The power of the turbopump is determined from the propellant mass and combustion chamber pressure, and based on this, the mass of the turbopump is determined. In addition, the flowrate of the turbine and GG are determined from the power of turbopump, which determines the GG mass and additional propellant for driving the pump. Since the specific impulse is obtained by dividing the mass flowrate to thrust level, loss of specific impulse occurs due to the additional propellant required to drive the pump in the GG cycle.

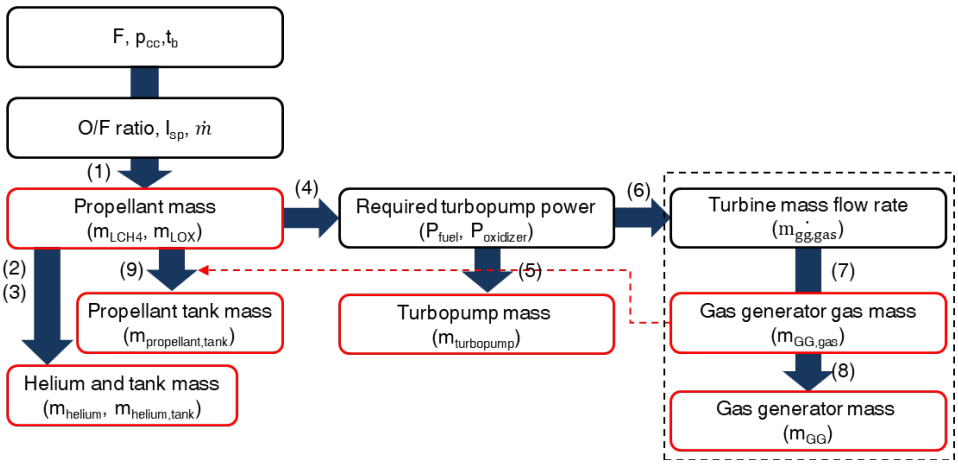

Figure 3.1 Mass modeling of the GG cycle

(1) $m_{LCH4,cc} = \dot{m}t_b \frac{1}{O/F+1}$, $m_{LOX,cc} = \dot{m}t_b \frac{O/F}{O/F+1}$

(2) $m_{helium} = \kappa_u \kappa_h \frac{k_h}{R_h T_0} \frac{p_{LCH4} V_{LCH4} + P_{LOX} V_{LOX}}{1 - p_h^1/p_h^2}$

(3) $m_{helium,\,tank} = \frac{3}{2} \kappa_u \kappa_h \kappa_{tank} \frac{\rho_{tank} k_h}{\sigma_{tank}} \frac{p_{LCH4} V_{LCH4} + P_{LOX} V_{LOX}}{1 - p_h^1/p_h^2}$

(4) $P_{pump} = P_{pump,LCH4} + P_{pump,LOX} = \frac{\Delta p_{LCH4} \dot{m_{LCH4}}}{\rho_{LCH4} \eta_{LCJH4}} + \frac{\Delta p_{LOX} \dot{m_{LOX}}}{\rho_{LOX} \eta_{LOX}}$

(5) $m_{turbopump} = 2.6 \times (\frac{P_{turbopump}}{RPM * 0.10472})^{0.667}$ [12]

(6) $P_{pump} = P_{turbine} = \eta_{turbine} C_{p,gg,gas} \dot{m_{gg,gas}} T_{turbine} \left(1 - p_{turbine,ratio}^{(1-k_{gg})/k_{gg}}\right)$ [13]

(7) $m_{LCH4,gg} = \dot{m_{gg,gas}} t_b \frac{1}{O/F+1}$, $m_{LOX,gg} = \dot{m_{gg,gas}} t_b \frac{O/F}{O/F+1}$

(8) $m_{gg} = \frac{3}{2} \frac{\kappa_{gg} \rho_{gg} p_{gg,gas}}{\sigma_{gg}} V_{gg,gas}$

(9) $m_{LCH4,\,tank} = \frac{3}{2} \kappa_u \kappa_{tank} \frac{\delta_{tank} p_{tank}}{\sigma_{tank}} \frac{m_{LCH4,cc} + m_{LCH4,gg}}{\rho_{LCH4}}$

3.2 Electric pump cycle

As shown in Figure 3.2, the mass modeling of the EP cycle is generally similar to that of the GG cycle modeling. However, the process of obtaining the turbine and GG from the power of the pump has been replaced by the motor/inverter/battery mass. The process of calculating the mass of the motor, inverter, and battery is calculated using the power density representing the weight of the power as in Equations 6 and 7. On the other hand, due to the weight of the electrical components, the drying weight was higher than the GG cycle.

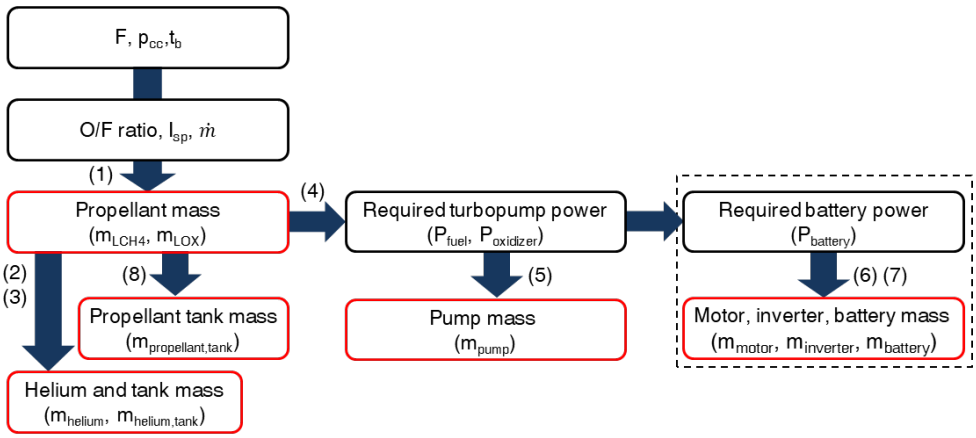

Figure 3.2 Mass modeling of the EP cycle

(1) $m_{LCH4,cc} = \dot{m} t_b \frac{1}{O/F+1}$, $m_{LOX,cc} = \dot{m} t_b \frac{O/F}{O/F+1}$

(2) $m_{helium} = \kappa_u \kappa_h \frac{k_h}{R_h T_0} \frac{p_{LCH4} V_{LCH4} + P_{LOX} V_{LOX}}{1 - p_h^1 / p_h^2}$

(3) $m_{helium,\,tank} = \frac{3}{2} \kappa_u \kappa_h \kappa_{tank} \frac{\rho_{tank} k_h}{\sigma_{tank}} \frac{p_{LCH4} V_{LCH4} + P_{LOX} V_{LOX}}{1 - p_h^1 / p_h^2}$

(4) $P_{pump} = P_{pump,LCH4} + P_{pump,LOX} = \frac{\Delta p_{LCH4} \dot{m_{LCH4}}}{\rho_{LCH4} \eta_{LCJH4}} + \frac{\Delta p_{LOX} \dot{m_{LOX}}}{\rho_{LOX} \eta_{LOX}}$

(5) $m_{turbopump} = 2.6 \times \left(\frac{P_{turbopump}}{RPM * 0.10472}\right)^{0.667}$

(6) $m_{motor} = \frac{P_{pump}}{\delta_{notor}}$, $m_{inverter} = \frac{P_{pump}}{\delta_{inverter} \eta_{motor}}$

(7) $m_{battery} = \frac{\kappa_{battery} P_{pump}}{\delta_{inverter} \eta_{motor} \eta_{inverter}}$ or $\frac{\kappa_{battery} P_{pump}}{\varepsilon_{battery} \eta_{battery} \eta_{motor} \eta_{inverter}} t_b$

(8) $m_{LCH4,\,tank} = \frac{3}{2} \kappa_u \kappa_{tank} \frac{\delta_{tank} p_{tank}}{\sigma_{tank}} \frac{m_{LCH4,cc}}{\rho_{LCH4}}$

3.3 Pressure-fed cycle

Figure 3.3 shows the mass modeling of the pressure-fed cycle. It consists only of fuel, fuel tank, helium, and helium tank. Based on the given engine thrust, combustion chamber pressure, and combustion time, the propellant mass can be calculated as shown in Equation 1. In addition, assuming adiabatic expansion through propellant mass and initial pressure of helium, helium mass and helium tank mass can be calculated as in Equations 2 and 3. Finally, the propellant tank must be pressurized at a pressure higher than the combustion chamber pressure, and the mass of the propellant tank can be obtained using the pressure and yield strength as shown in Equation 4.

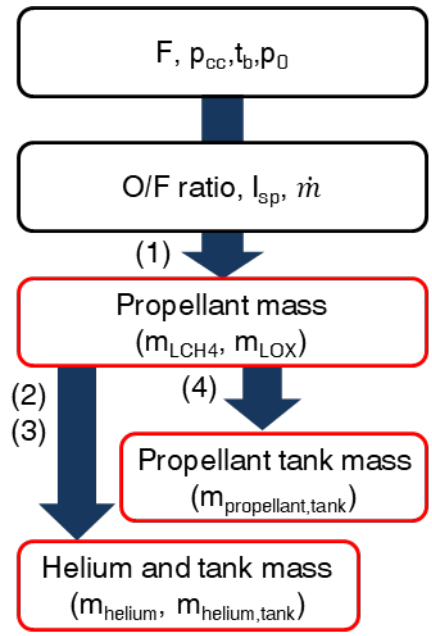

Figure 3.3 Mass modeling of the pressure-fed cycle

(1) $m_{LCH4} = \dot{m} t_b \frac{1}{O/F+1}$, $m_{LOX} = \dot{m} t_b \frac{O/F}{O/F+1}$

(2) $m_{helium} = \alpha \kappa_{p1} \kappa_u \kappa_h \frac{\gamma_h M_h}{R_h T_0} \frac{m_p p_{cc}}{1-\kappa_{p1} p_{cc}/p_0}$

(3) $m_{helium,\,tank} = \frac{3}{2} \alpha \kappa_{p1} \kappa_u \kappa_h \kappa_{tank} \gamma_h \frac{\rho_{tank}}{\sigma_{tank}} \frac{m_p p_{cc}}{1-\kappa_{p1} p_{cc}/p_0}$

(4) $m_{LCH4,\,tank} = \frac{3}{2} \alpha_{LCH4} \kappa_{p1} \kappa_u \kappa_{tank} \frac{\delta_{tank}}{\sigma_{tank}} m_p p_{cc}$

3.4 Results and discussion

In the pump design process, specific speed (n_s) is dimensionless number used to predict pump performance and efficiency and related to geometry of the pump [14]. In general, for the low specific speed, the lower the specific speed, the lower the hydraulic efficiency of the pump. Figure 3.4 shows the efficiency of the pump according to the specific speed which is empirical data.

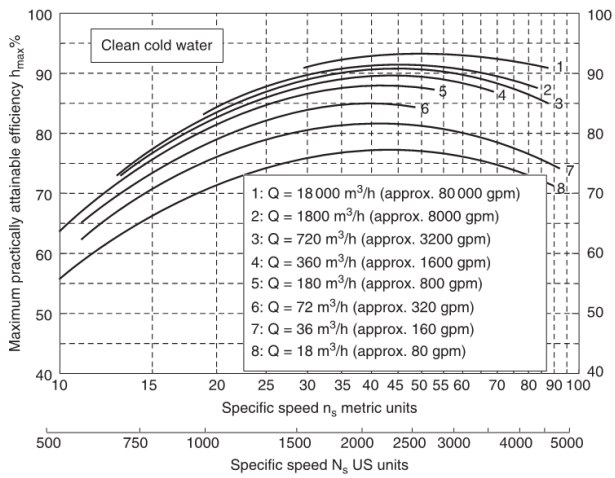

Figure 3.4 Efficiency of the pump according to the specific speed

In general, the pump with the ns under 500 in U.S unit is impractical [15]. The empirical expression of the efficiency over the specific speed is as follows [16].

$$\eta_{pump} = 0.94 - 0.08955 \times \left[\frac{Q(gpm)}{N(rpm)} \times X\right]^{-0.21333} - 0.29 \times [\log_{10}\left(\frac{2286}{N_s}\right)]^2$$

At the same combustion chamber pressure and rotational speed, as the thrust decrease, the specific speed and efficiency also decrease. At the same rotational speed, the specific speed decreases as the combustion chamber pressure increases. Figure 3.5 shows the specific speed and efficiency of the fuel pump. Figure 3.6 shows the specific speed according to the thrust.

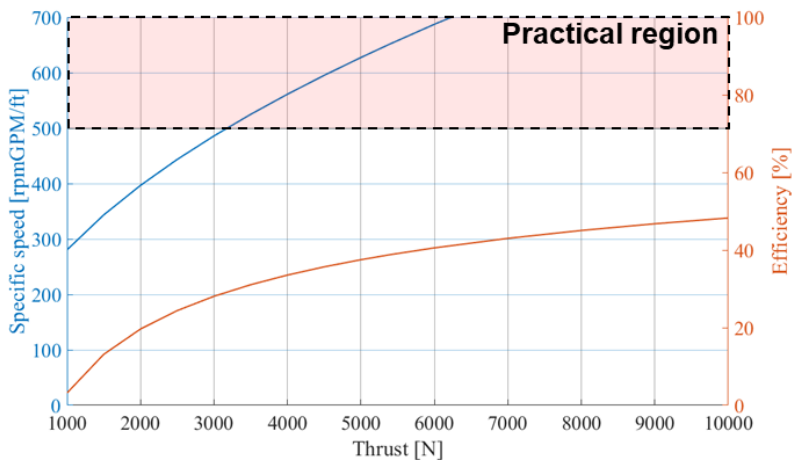

Figure 3.5 Specific speed and efficiency of the fuel pump according to the thrust (N=28000 RPM, P_{cc}=10 bar)

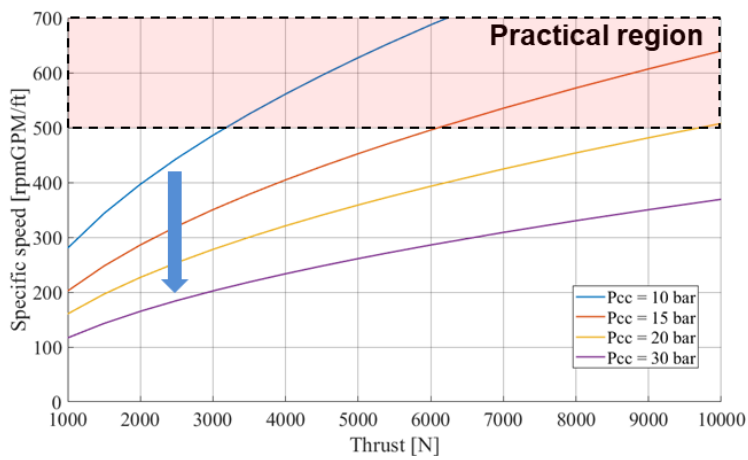

Figure 3.6 Specific speed according to the thrust (N=28000 RPM)

Figure 3.7, Figure 3.8, and Figure 3.9 present the initial mass budgets of the GG cycle, EP cycle, pressure-fed cycle, respectively. Condition of mass modeling is as follows: The thrust level, combustion chamber and pump rotational speed are 5.4 kN, 20 bar, 28000 RPM, respectively.

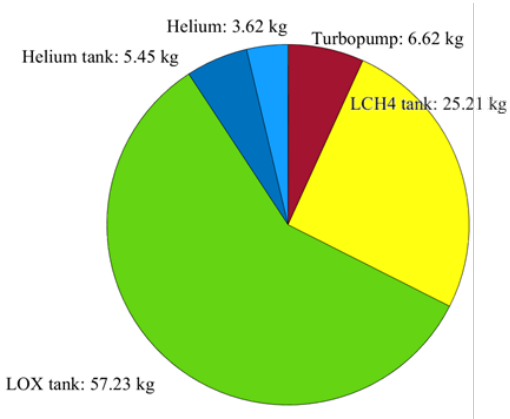

Figure 3.7 Initial mass budget of the GG cycle

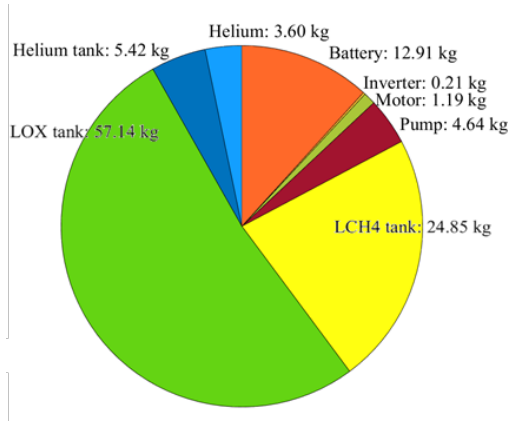

Figure 3.8 Initial mass budget of the EP cycle

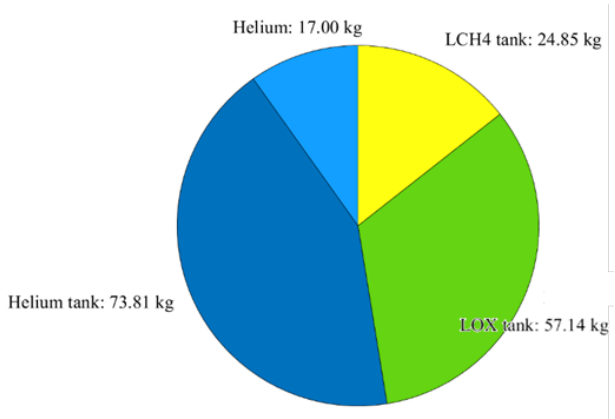

Figure 3.9 Initial mass budget of pressure-fed cycle

The payload mass was calculated as a condition for Vega's three-stage engine, a small European launch vehicle [17]. The combustion time is 500 seconds, and the speed increment is 1500 m/s. Under conditions of a combustion chamber pressure of 10 bar, a pump rotation speed of 28000 RPM, and a thrust of 5.4 kN, the EP cycle has lowest both dry and wet mass, and the GG cycle has highest both dry and wet mass. Finally, the payload mass representing the performance of the propellant feed system was better in the EP cycle than in the GG cycle and the pressure-fed cycle. Figure 3.10 presents and system mass budget of the GG cycle, EP cycle and the pressure-fed cycle. Figure 3.11 presents performance comparison between three propellant feed system.

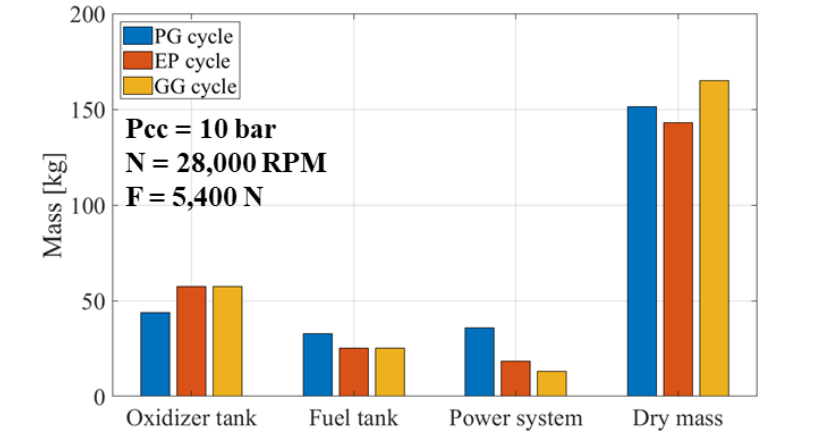

Figure 3.10 System mass of GG cycle, PG cycle and EP cycle

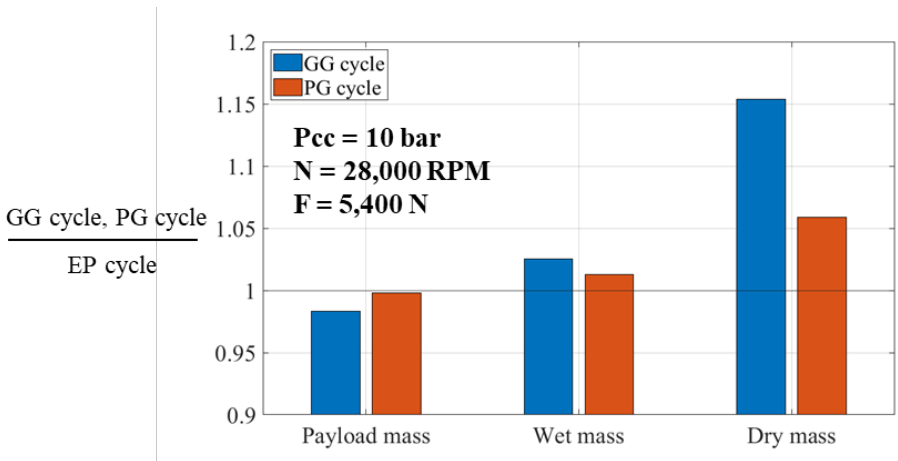

Figure 3.11 Performance comparison between GG cycle, EP cycle and pressure-fed cycle

Figure 3.12 shows the specific impulse and O/F ratio of the EP cycle and the GG cycle according to the combustion chamber pressure. The higher the combustion chamber pressure, the greater the amount of additional propellant consumed by the GG and turbine of the GG cycle. Thus, the higher the combustion chamber pressure, the lower the specific impulse of the GG cycle.

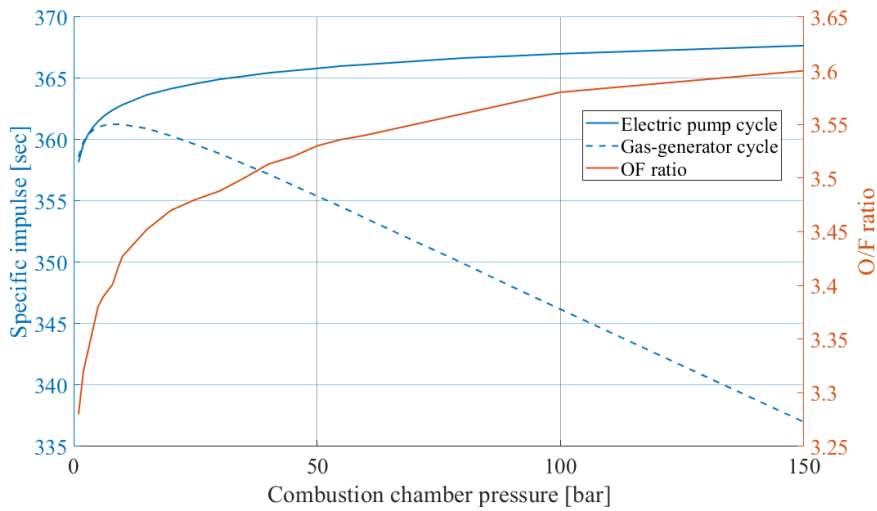

Figure 3.12 Specific impulse and O/F ratio of the EP cycle and the GG cycle according to combustion chamber pressure

A proper feed system for the small rocket engines is derived based on the results of the mass modeling of three propellant feed system. Figure 3.13 shows the practical region of the propellant feed system according to the thrust level and combustion chamber pressure when the pump rotational speed is 28000 RPM. For the high thrust, pressure-fed cycle has lowest performance. Even at combustion chamber pressure above 47 bar, the payload mass becomes negative. This means that the pressure-fed cycle is not applicable to a rocket engine with the combustion chamber pressure condition of 47 bar or more. Performance of the GG cycle is similar with the EP cycle. However, for the thrust level under 10000 N, the dominant region of the EP cycle is wider than the GG cycle.

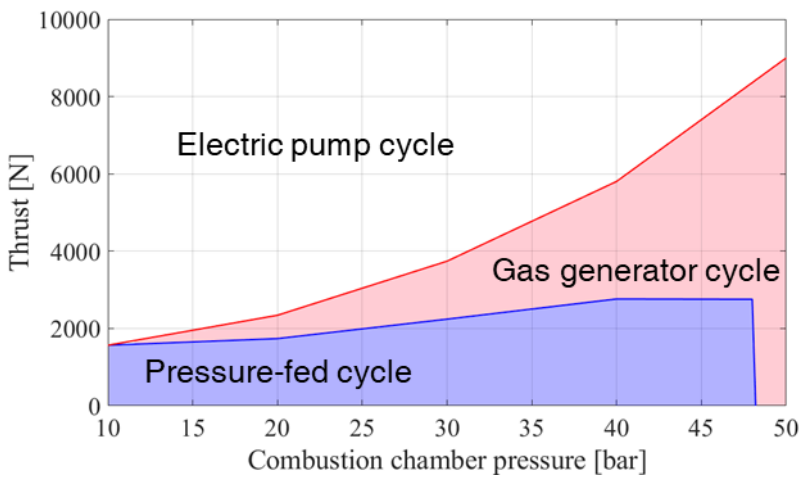

Figure 3.13 Practical region of the feed system according to thrust and P_{cc} (N = 28000 RPM)

Chapter 4. CONCLUSION

In this study, the performance of the EP cycle with low thrust level was evaluated based on the mass modeling. At the design conditions, rotational speed of 28000 RPM, thrust of 5,400 N and the combustion chamber pressure of 10 bar, the performance of the EP cycle was the best option compared to the GG cycle and the pressure-fed cycle. In addition, the pump was successfully operated to the cryogenic rotational speed, and hydroelectric performance tests were performed at 10000 RPM and 14000 RPM. In addition, numerical analysis modeling was performed based on the performance test results, and performance in real propellant was predicted through numerical analysis.

This study revealed that the EP cycle could be the best option for small launch vehicles with payload performance of less than 300 kg. In terms of qualitative aspects, the EP cycle becomes easy to control the thrust of a pump because of a simple pump rotation speed control, and thus could be used for reuse and increase the accuracy of input of payload orbit. In terms of quantity, the electric pump cycle had a higher payload weight that satisfies the same speed increment.

There are two limitations of this study. First, the mass of the GG predicted based on the current stress and yield strength is only 40 g in a 5.4 kN-class rocket engine, which is not reasonable. Therefore, it seems that mass modeling needs to be improved. Second, there was a lack of academic approach to the occurrence of differences in performance due to the viscosity of liquid nitrogen and thermodynamic effects. In the future, we plan to design an electric pump for oxidants using liquid methane and a numerical analysis model. In addition, as mentioned in the limitations, we would like to approach system mass modeling from a more realistic perspective.

Bibliography

[1] Liu, Y., Yang, J., He, Y., Ni, Z., Wu, Y. Concept and key technology analysis of electric-pump-fed liquid propellant rocket engine. IOP Conference Series: Earth and Environment Science. 2021, 781.

[2] Kwak, H.D., Kwon, S., Choi, C.H. Performance assessment of electrically driven pump-fed LOX/kerosene cycle rocket engine: Comparison with gas generator cycle. Aerospace Science and Technology. 2018, 77: 67–82.

[3] Lee, J., Roh, T.S., Huh, H., Lee, H.J. Performance analysis and mass estimation of a small-sized liquid rocket engine with electric-pump cycle. International Journal of Aeronautical and Space Science. 2021, 22, 94–107.

[4] Cui, P., Li, Q., Cheng, P., Chen, L. System scheme design for LOX/LCH4 variable thrust liquid rocket engines using motor pump. Acta Astronautica. 2020, 171, 139–150.

[5] Liang, T., Song, J., Li, Q., Cui, P., Cheng, P., Chen, L. System scheme design of electric expander cycle for LOX/LCH4 variable thrust liquid rocket engine. Acta Astronautica. 2021, 186, 451–464.

[6] Casalino, L., Maseeni, F., Pastrone, D. Viability of an electrically driven pump-fed hybrid rocket for small launcher upper stages. Aerospace. 2019, 6, 36.

[7] Rachov, P.A., Tacca, H., Lentini, D. Electric feed system for liquid-propellant rockets. Journal of Propulsion and Power. 2013, 29, 1181-1180.

[8] Yoon, J. A study on the design of electric pump for small liquid methane rocket engine, Master's Thesis, Seoul National University, 2020.

[9] Kim, D. An investigation on impeller design of electric pump cycle for lander rocket engine. Master's Thesis, Seoul National University. 2021.

[10] Park, Y.K., Kim, D., Yoon, J., Jeong, G., Yoon, Y. Hydraulic performance test of electric pump for small methane rocket engine. The Korean Society for Aeronautical & Space Science, Autumn Conference. 2020, 511-512.

[11] Kim, H.K., Kwak, H.D., Choi, C.H. Kim, J. Conceptual design of electric-pump motor for 50kW rocket engine. Journal of The Korean Society for Aeronautical and Space Sciences. 2018, 46, 2, 175-181.

[12] Karaveckas, L. Development of low-cost pressurization system for rocket engines. Ph.D thesis, Kingston University, 2019.

[13] Sutton, G.P., Biblarz, O. Rocket Propulsion Elements, eighth edition., Wiley, New York, 2010.

[14] Gulich, J.F., Centrifugal pump in 2nd edition, Springer, 2010.

[15] Hiroshi, S., Kazuo, U., Yinchun, C. Designing an ultra-low specific speed centrifugal pump. Proceedings of the 22th International Pump Users Symposium. 2005, 16–21.

[16] Karassik, I.J., Messina, J.P., Cooper, P., Heald, C.C. Pump Handbook, McGraw-Hill, New York, NY, USA, 3rd edition, 2001.

[17] Ballard, C. Conceptual lay-out of a Small Launcher. Master's Thesis, ISAE-ENSICA. 2012

초 록

인공위성의 소형화 및 군집 시스템의 활용이 증가함에 따라 소형 발사체에 대한 수요도 늘어나고 있다. 이에 따라, 수많은 민간 기업에서 소형 발사체를 개발 및 운용하고 있으며, 특히 전기펌프 사이클을 적용한 소형 발사체들이 증가하고 있는 추세이다. 전기펌프 사이클은 가스터빈으로 펌프를 구동하는 가스 발생기 사이클과는 달리, 전기모터를 사용하여 펌프를 구동하는 연료 공급 시스템이다. 질량 모델링을 통해 전기펌프 사이클과 다른 연료 공급 시스템과 비교하여 전기펌프 사이클의 성능을 평가하는 연구가 많이 이루어져 왔다. 하지만 10 kN 급 이하의 소형 로켓엔진에서 전기펌프 사이클 적용에 대한 타당성을 검토한 연구는 이루어지지 않았다. 본 연구에서는 실험 및 수치적인 방법으로 전기펌프 사이클 적용에 대한 타당성을 다루었다. 첫째, 5.4 kN 급 극저온 전기펌프 시스템을 설계하여 액체질소를 매질로 한 극저온 성능 시험을 수행했다. 수치 해석과 극저온 성능 시험 결과로부터 극저온 환경에서 전기펌프의 정상적인 작동을 확인했다. 둘째, 질량 모델링을 기반으로 전기펌프 사이클, 가스발생기 사이클, 가압식 사이클의 성능을 비교 및 분석했다. 10

kN 급 이하의 소형 로켓엔진은 작은 추력으로 인해 펌프의 비속도가 매우 낮다는 특징이 있다. 본 연구에서는 비속도에 따른 펌프의 수력학적 효율을 고려하여 질량 모델링을 수행했으며, 소형 로켓엔진에서 연소압, 추력, 펌프의 회전속도 조건에 따른 연료 공급 시스템의 성능을 비교했다. 실험적 타당성 연구에서 사용한 10 bar 의 연소압, 5.4 kN 의 추력, 28,000 RPM 의 펌프 회전속도 조건에서, 전기펌프 사이클의 성능이 다른 두 연료 공급시스템보다 높았다. 최종적으로 본 연구에서는 10 kN 급 이하의 소형 로켓엔진에서 전기펌프 사이클 적용의 타당성을 수치적으로 검증하였으며, 5.4 kN 급 소형 로켓엔진에서 전기펌프 사이클 적용이 가능함을 실험적으로 검증하였다.

주요어 : 전기펌프 사이클, 액체 메탄, 로켓 엔진, 극저온 시험, 수치 해석, 성능 평가

학번 : 2020-25188